Proceedings of ASME Turbo Expo 2011
GT2011
June 6-10, 2011, Vancouver, British Columbia, Canada

GT2011-45281

INVESTIGATION OF UNSTEADY COMPRESSOR FLOW STRUCTURE WITH TIP INJECTION USING PARTICLE IMAGE VELOCIMETRY

Roland Matzgeller
MTU Aero Engines GmbH
Munich, Germany

Melanie Voges
German Aerospace Center (DLR)
Cologne, Germany

Michael Schroll
German Aerospace Center (DLR)
Cologne, Germany

ABSTRACT

Fluid injection at the tip of highly loaded compressor rotors is known to be very effective in suppressing the onset of rotating stall and eventually compressor instability. To understand the effects of tip injection, the flow field at the tip region of a transonic compressor rotor with and without fluid injection was investigated in this paper. Using results acquired by phase-locked PIV measurements as well as the static pressure field obtained by fast response pressure transducers, the unsteady interaction between the injection jet and the rotor could be described thoroughly. Both, an influence of the rotor's flow field on the jet as well of the jet on the rotor was clearly visible. Since unsteady inflow conditions to the front rotor in the relative frame of reference were imposed by the injection jets, the rotor's unsteady response was investigated by inspection of the position of the tip leakage vortex trajectory. It could be shown that due to a short time for the flow to adapt at the rotor's leading edge, its position didn't change distinctly. Because a significantly longer time was needed for the overall passage flow to adapt, it was concluded that this causes the beneficial effect of tip injection.

INTRODUCTION

In an effort to cope with the rising demand to reduce fuel burn as well as the emission of NO_x and CO_2, along with research on new aero engine concepts [1], component efficiencies for modern aero engines have to be increased [2]. Particularly during the design phase of high pressure compressors, optimization of design point efficiency often leads to a decreased stable operating range at part speed conditions. In order to ensure sufficient stability margin throughout the compressor's operating range, methods to enhance stability have been under research since the early days of compressor development. Along with casing treatment, tip injection seems to be a promising attempt to stabilize the compressor and is thus part of the research program NEWAC which funded the investigations presented in this paper. At part speed conditions, where the tip sections of front rotors tend to trigger surge, both methods are beneficial for secondary flow areas near the outer casing, resulting in an enhanced stable operating range. Contrary to casing treatment, which is a permanent modification of the casing employing grooves or slots, tip injection consists of few small nozzles distributed over the circumference, which do not interact with the main flow.

Tip injection has been in focus of many research works where its influence on the compressor's or rotor's time averaged performance, which is represented by overall or stage characteristics, was investigated. Apart from pulsed injection, which is often coupled with a feedback control system and not under consideration in this paper, Suder et al. [3] first investigated steady tip blowing thoroughly. Varying the injection mass flow rate, injection velocity and number of injectors, they concluded that range extension correlated best with injection velocity, thus defining a mass averaged axial velocity. Above a certain number of injectors, range extension was virtually independent of it, even if the pattern was changed by clustering the nozzles. Unfortunately, no sound explanations of these effects were given. Cassina et al. [4] based their work on findings by Suder et al. They performed numerical parametric studies, investigating the influence of circumferential coverage as well as radial and circumferential injection angle. Without giving detailed explanations, they concluded that range extension was a function of both the circumferential coverage and the injection angle.

Although not investigated in literature yet, the results presented above suggest that range extension may be linked to unsteady flow effects. With discrete tip injection, a pattern where an injection jet is followed by undisturbed flow appears near the casing, i.e. over the radial extend of the injection jet. Thus, in the rotating frame of reference unsteady inflow conditions are generated for the rotor. Since several authors [3], [4], [5] confirm that range extension correlates with circumferential coverage of nozzles and injection velocity it is likely that unsteady flow plays a major role in determining the range extension.

As a first step to inspect unsteady flow at the rotor's tip region with discrete tip injection, this paper investigates the unsteady inflow conditions generated by the discrete jets as well as the unsteady movement of the tip leakage vortex, which is commonly related to the development of rotating stall [10]. Phase-locked Particle Image Velocimetry (PIV) measurements were carried out to record the unsteady velocity field at the rotor's tip. Unsteady pressure transducers, applied at the casing complemented the picture by providing static pressure information which is crucial in determining the nozzles' exit conditions.

NOMENCLATURE

chord	C
normal strain rate: $\frac{\partial u}{\partial x}+\frac{\partial v}{\partial y}$	ε_1
shear strain rate: $\frac{\partial u}{\partial y}+\frac{\partial v}{\partial x}$	ε_2
camera focal length	f
reduced mass flow rate	m_{red}
reduced rotational speed	N
total pressure ratio	Π
phase angle	Φ
radius	r
tip clearance height	τ
circumferential absolute velocity component	u
axial absolute velocity component	v
coordinate along rig axis	x
coordinate in circumferential direction	y

Subscripts

conditions at aerodynamic design point	A
normalized value	norm

DESCRIPTION OF TEST CONFIGURATION

Test compressor and fluid injection system

Fluid injection was tested on a high pressure compressor, where the casing above the first rotor was modified, in order to contain the injection nozzles. The compressor is a multi stage high pressure compressor with three variable guide vanes (an IGV and two variable stator vanes). The compressor's front rotor is transonic at design conditions but subsonic all over the span at part speed, i.e. at N/N_A = 90%, where all measurements were taken. At this speed the relative measured tip clearance height τ/C equals 0.46%. Six injection nozzles, equally spaced around the circumference, were placed upstream of the first rotor, i.e. between the IGV and the first rotor. The nozzles are inclined to the rig axis by 45° and cover 10% of the circumference, i.e. the ratio between the circumference covered by the injection jets and the whole circumference is 10%. An injection system rather than a recirculation system was chosen to feed the nozzles, which allowed to control the injected mass flow rate independently from the compressor's operating conditions, using adjustable valves. Inlet total temperature and total pressure were measured by traverses upstream the IGV, i.e. at the compressors inlet. Stage performance was then calculated using stator leading edge instrumentation and static pressure measurements downstream the stator row.

More information about the injection system, the test compressor, and its instrumentation can be found in Hiller et al. [5], who used the same compressor to investigate overall performance with and without tip injection. In order to explore the unsteady flow field between the injection channel and the first rotor by PIV measurements, optical access had to be provided. Thus, an injection nozzle geometry different to the one used in [5] was employed. Nevertheless, apart from the injection nozzles, the rest of the test configuration remained unchanged compared to [5].

Unsteady instrumentation

Along with the PIV system, which will be depicted in detail in the subsequent section, an array of 16 unsteady wall bounded static pressure transducers was placed upstream of the first rotor. The same relative position as between injection nozzle exit and the optical access for PIV was chosen for this array, which allowed acquiring velocity information (via the PIV system) and static pressure information simultaneously.

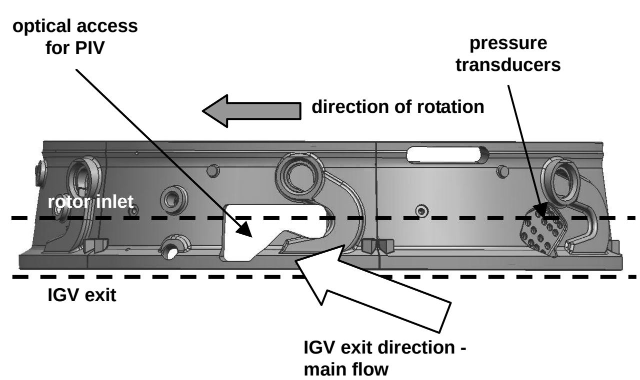

Fig. 1 Top view onto casing

Fig. 1 shows a top view onto the casing, where both the optical access necessary for PIV measurements as well as the array of static pressure transducers is visible. Additionally, two dashed lines are plotted, which indicate the positions of the rotor inlet and the IGV's outlet at the tip, respectively. Since the array of pressure transducers is shifted a sufficiently long distance against the sense of rotation relative to the PIV measurement volume, any influence on PIV measurements is omitted. A sampling rate of 204.8 kHz provides sufficient resolution to capture pressure variations associated with the rotor, as it allows for 30 time discrete points per pitch at a speed of N/N_A = 90%. The pressure signal itself is filtered by a low-pass filter of 80 kHz to diminish aliasing effects. By combining these 16 probes it is possible to get a footprint of the unsteady rotor static pressure field at the casing, which is important in order to assess the nozzles' unsteady outlet conditions.

In addition to the array of 16 static pressure transducers, 6 wall bounded static pressure probes, equally spaced at the circumference and having the same sampling and filtering rate as sensors used for the matrix described above, were placed over the rotor leading edge. These probes were used to identify the occurrence of rotating stall and complemented the picture gained by the matrix of 16 pressure probes.

DESCRIPTION OF PIV MEASUREMENTS

Testcase and setup

As was already motivated in the previous section, sufficient optical access had to be provided for both, laser light sheet and camera window. Therefore, in addition to an adapted channel design, some modifications to the compressor casing were in need.

Fig. 2 shows the revised injection flow path designed such that optical access was possible between the nozzle's exit and the first rotor's leading edge.

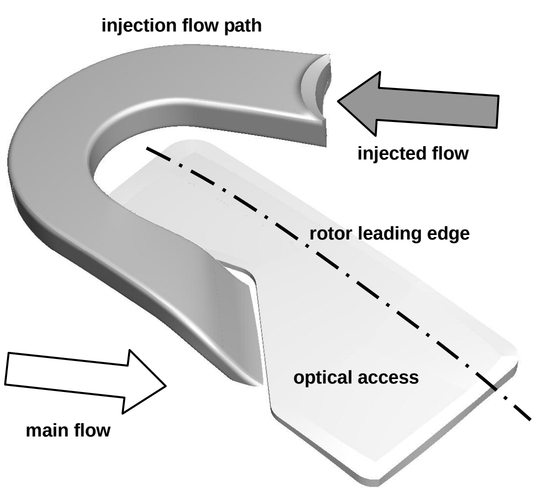

Fig. 2 Geometry of the injection flow path and the optical access

The flow path was bent around the casing opening, in order to guarantee optical access for a camera, which recorded the displacement of particles from outside the compressor, necessary for PIV. Similarly to [5], the flow path employed a very shallow angle with respect to the casing, in order to profit from the Coanda effect, generating a wall bounded injection jet. Consequently, all nozzles were flush with the casing wall and did not protrude into the flow path. Pre-design calculations with CFD were performed to ensure a separation free channel and eventually uniform flow conditions at the nozzle's exit.

Due to the complex geometry of the tip injection system, the observation window was suitably milled to precisely match the inner contour of the casing and the injection channels. To prevent the quartz glass window from any possible damage caused by mechanical stresses, a thin silicone sealing was applied between window support and glass. The geometry of the observation window and the related window support which precisely fits into the casing opening is given in Fig. 3.

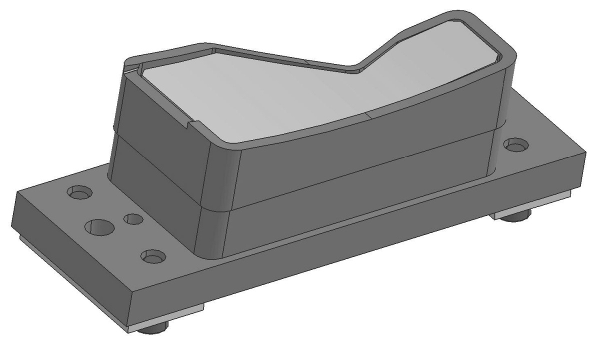

Fig. 3 Window support and quartz glass window

The laser was delivered into the measurement section using a specific periscope-type light sheet probe, designed at DLR's Engine Measurement Department. The concept of the probe allowed for near-wall PIV investigation with minimal aerodynamic impact on the flow structures under observation. This was achieved by small probe diameter of 12 mm and integrating the probe into a recess cavity in the axial gap between IGV and rotor, as shown in Fig. 4.

The height of the recess cavity determined the maximum distance Δz between the light sheet was traversed, in order to record the flow field at different radial positions. The probe itself contained very small optical components with diameters below 6 mm that required a precise alignment of the laser beam path through the probe, to avoid streaking and associated laser flare from the inner surface of the beam guiding tube. The light sheet was formed using a set of collimating lenses for laser beam diameter adjustment, combined with two different cylindrical lenses with orthogonal focus planes, resulting in a light sheet divergence angle of 25° and a thickness of 2.5 times the tip clearance height τ. A mirror in the head of the periscope probe deflected the light sheet by 90° into the blade passage. The desired measurement planes were adjusted by traversing the probe in height and aligning the light sheet with a calibration target attached to an additional window support prepared for light sheet and camera alignment. To prevent possible deposits of aerosol seeding or dust on and subsequent damage to the exposed optical surfaces, the light sheet probe was purged with dry, clean, and oil-free air. Direct laser reflection from the blade surfaces could be reduced by covering the entire first rotor, i.e. both the blades as well as the rotor's hub, with a thin layer of black anti-reflective paint.

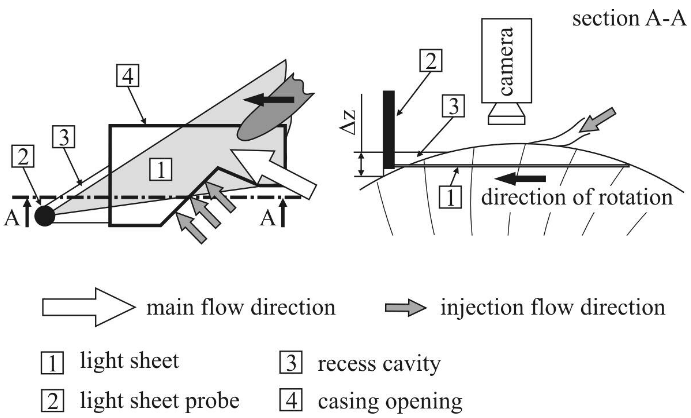

Fig. 4 Details of PIV setup

PIV measurement system

To illuminate the tracer particles in the light sheet a commonly available Nd:YAG PIV laser system (532 nm wavelength) with two resonators provided double pulses around 50 mJ per pulse at a repetition rate of 15 Hz. The laser beam was guided via an articulated mirror arm from the vibration-sensitive laser head to the light sheet probe, which was fixedly mounted to the casing (see Fig. 4). Thus any machine vibrations or movement did not affect the carefully adjusted light sheet position relative to the casing and additionally prevented the laser head from any damage or misalignment.

Tracer particles were generated by means of a smoke generator that operated on an evaporation-condensation principle and yielded smoke particles in the range of 300 to 800 nm. To achieve a homogeneous particle distribution the smoke was introduced upstream of the settling chamber in front of the inlet bellmouth, which provided very good and stable global seeding rates. The mean particle diameter was about 500 nm, thus a good response to the rotor flow field could be assured.

An additional seeding generator was needed for the tip injection system. Here an aerosol generator operated with a mixture of paraffin oil and ethanol was used. The liquid was dispersed using a set of sonic nozzles and pressurized air at 12 bar. While the ethanol evaporates the remaining paraffin oil particles were carried with the air flow passing another sonic orifice to collect the fraction of undesired larger particles before the seeding was fed into the measurement section. The final particle diameter was in the order of 500 nm.

For flow observation a thermo-electrically cooled, double-shutter CCD camera with a maximum frame rate of 15 Hz at a spatial resolution of 2,048 x 2,048 pixels was used. Due to the special window geometry the active area of the sensor could be reduced to 2,048 x 1,024 pixels yielding a final magnification factor of 27 pixel/mm. The camera was mounted on a three-axis remote-controlled traversing unit to optimize camera positioning during the experiment. The focal length of the chosen camera lens was $f = 100$ mm. The camera object plane was aligned with the light sheet plane using the afore mentioned calibration target, equipped with a precise 2 x 2 mm² dot grid. A narrow band pass filter prevented the camera lens from collecting interfering environmental light and hereby over-illuminating the CCD sensor during image acquisition.

Data acquisition and post processing

For synchronization of the laser pulses with the camera exposure times a programmable sequencer unit was used, which also allowed the adjustment of the time interval between both laser pulses, so-called pulse distance. In the case of the measurements conducted during this test campaign, a pulse distance of 1.0 µs was employed, which bespeaks a laser pulse distance of 0.6% of the rotor pitch movement for the given rotational speed at $N/N_A = 90\%$. The rather low PIV acquisition rate of 15 Hz was insufficient for directly resolving typical flow structures at the blade passing frequency (BPF). Therefore a rotor blade trigger signal was fed into a phase-shifting unit and triggered phase-constant PIV measurements. Starting from a well-defined reference position the phase angle Φ was increased in 8 equidistant steps per blade pitch for all measurement planes and operation conditions.

At some rotor positions the light sheet impinging on the moving blades resulted in laser flare and subsequently caused overexposure of the CCD sensor in the vicinity of the blade (so-called image blooming). This image area could not be used for evaluation and therefore was covered with a mask to speed up image post-processing. The same procedure applied for other image areas without velocity information, e.g. window brace or parts of the rotor blades. For each phase angle a PIV data set of 500 instantaneous double-images was recorded and stored on a PC for subsequent evaluation.

Image dewarping was applied in order to reduce the lensing effects caused by the inner curvature of the glass window. Calculation of the velocity fields was performed applying a cross-correlation algorithm including grid refinement, starting with an interrogation window size of 32 x 32 pixels and a final window size of 16 x 16 pixels using 50% overlap. This resulted in a final grid size of the velocity vector maps of 0.3 x 0.3 mm². More details on the processing methods can be found in Raffel et al. [6]. Sub-pixel accuracy was accounted for applying image-shifting routines with the Whittaker approach as peak fitter ("sinc"-kernel interpolation [7]). Outlier detection was based on normalized median filtering [8]. The mean number of detected outliers was in the order of 10% of the entire vector field. About two thirds of the rejected vectors could be validated by taking into account lower order signal peaks of the related cross correlation. The remaining spurious vectors, about 3.4% of the entire vector field, were replaced by linear interpolation. For the calculation of the phase-averaged velocity fields all 500 instantaneous PIV velocity maps were considered.

Finally it should be noted that the present PIV measurements only captured the projection of the three dimensional velocity vectors onto the light sheet plane under observation, i.e. velocity components u and v. Therefore the out-of-plane component was not detectable with this single-camera setup.

In addition to the velocity information in the light sheet plane, other flow quantities such as normal and shear strain rate (ε_1 and ε_2) could be derived from the two planar velocity components u and v. However, due to the a planar setup the strain tensor values involving the out-of-plane velocity component could not be determined and thus are not considered for calculation of the strain magnitude $|\varepsilon|$, which is important for the detection of vortices in the following.

Error analysis

Different error sources should be taken into account to quantify the order of magnitude of the possible error made during PIV data recording and post processing. Using state-of-the-art PIV processing routines and following the assessment made by Westerweel [8], a measurement error of 0.1 pixels can be assumed. In the present application a maximum pixel shift of 11 pixels at 100% rpm was present, corresponding to a relative measurement error of 0.9% of the full scale value (about 4 m/s in the absolute domain). The accuracy of the trigger unit to adjust the different rotor phase angles can be estimated to be 2.3% related to the chosen step size.

It has to be mentioned that these PIV measurements were not performed in a clean laboratory environment, but in a realistic compressor stage under challenging conditions. Therefore the theoretical error analysis underestimates the real measurement error. In this special case the quality of the acquired data was significantly depending on the operating conditions of the compressor stage (e.g. with/without tip injection, rotational speed). As the PIV measurements were chosen to be performed during the onset of rotating stall or in already separated flow conditions close to the casing, a considerable contamination of the observation window due to centrifuged seeding particles or condensation of air moisture had to be accepted.

Fig. 5 shows PIV raw data as recorded by the CCD camera. The grey scale has been inverted for better visibility (brightest areas appear black). The window area is indicated by a white bold line. Particles in the light sheet area 1 appear as black points and are used to gain velocity information, as stated above. However, also contaminations due to droplets or separated flow 4 along with laser reflections at the rotor's hub 3 are visible. Areas containing no flow information, i.e. areas of the image which cover parts of the casing 2 or the rotor blade 5, were masked (shown in blue). During data analysis it could be demonstrated that image areas with a poor data validation rate could be associated with local window contamination related to flow structures close to the casing (flow separation or re-attachment, see Fig. 5) or diffuse laser stray light from casing parts and the hub, respectively. This has been accounted for during image processing by choosing only locally working outlier detection routines (instead of global filtering). Thus, it was possible to obtain velocity information which was not influenced by local areas of contamination on the window. Areas of particular interest, such as the tip leakage vortex were therefore identifiable using velocity information at the measuring plane.

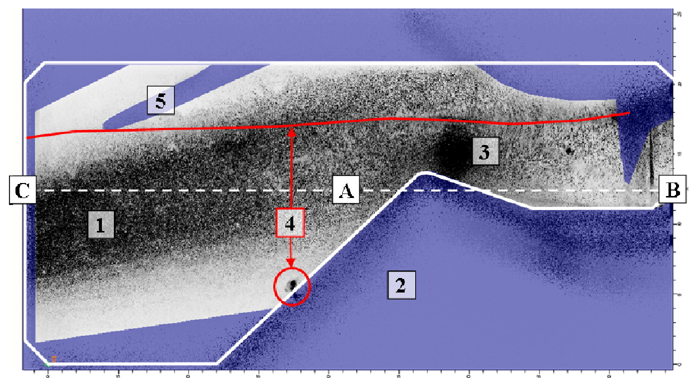

Fig. 5 PIV raw data after dewarping

In conjunction with the necessary image dewarping routines to correct for the window lensing effect the authors consider a reasonable measurement error to be in the order of 5% of the full scale value, which to the authors' knowledge is in good agreement with other turbomachinery related applications of PIV.

MEASUREMENT RESULTS

Tests were conducted at different part speeds as well as at design speed. However, since the interaction between the injection jet and the blade at highly throttled conditions was in focus for this paper, one particular test case, which is typical for an application of front stage fluid injection, was selected.

Both, PIV measurements as well as time averaged stage characteristics are presented at a relative reduced speed of $N/N_A = 90\%$. For PIV, the light sheet was fixed at a single radial position and spans a measuring plane (secant) which intersects the annulus at 96% of its height at the circumferential midpoint of the observation window (denoted as point A in Fig. 5). At both short edges of the observation window (points B and C in Fig. 5), the light sheet intersects the annulus at 98.5% height. Only one test case with injection, where 2.2% of the total inlet mass flow rate was injected, is considered in this paper. For this relative injection mass flow rate the injection jets cover 6.3% of the annulus height. Thus, the selected measuring plane intersects the injection jet, even at its lowest point, which is at the midpoint of the observation window.

Front stage behavior

In order to show the behavior of the front stage with and without tip injection at the selected reduced speed of $N/N_A = 90\%$, stage characteristics, given by the stage's total pressure ratio as a function of the reduced inlet mass flow rate, are presented in Fig. 6. Both characteristics have been normalized with the corresponding conditions at the operating point on the working line of the overall compressor. The control volume was chosen such that it encompasses the injection nozzles, which are placed upstream the rotor (see Fig. 1) as well as the front stage itself.

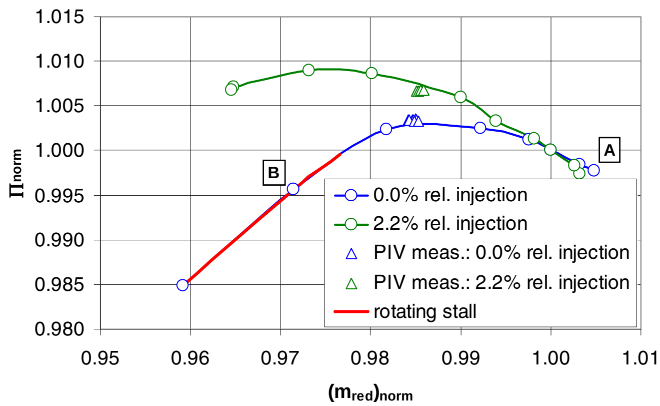

Fig. 6 Stage characteristics for cases with and without tip injection

It is evident from Fig. 6 that in case where tip injection was disabled, the front stage is highly throttled, identifiable by the front stage's characteristic which peaks and rolls over when throttling the compressor. However, due to a strong back-end, providing sufficient pressure build-up, the overall compressor sustains the back pressure imposed by the exit throttle and throttling beyond the peak of the front stage's characteristic is possible. As soon as the front stage has rolled over, rotating stall is present in the case where tip injection was disabled. The throttling range, where rotating stall could be verified by inspection of wall static pressure measurements at the front rotor's leading edge is indicated in red in Fig. 6.

Fig. 7 compares the power density spectra obtained by FFT analysis of these static pressure data recorded at operating points A and B, marked in Fig. 6. Frequency was normalized by the rotor revolution frequency, whereas amplitude was normalized by the peak amplitude, which occurs as soon as rotating stall is present. At the de-throttled point, i.e. at point A, only one distinct peak, which represents the rotor revolution frequency, is visible. However, as soon as the characteristic has rolled over, multiple stall cells are present, observable by peaks in the power density spectrum of point B at 77%, 154% and 231% of the rotor revolution frequency. These stall cells cluster to a single cell, encompassing the whole circumference near the overall compressor's stall point.

In the case where fluid was injected at a relative injection mass flow rate of 2.2%, operating behavior of the front stage changes drastically. Both, a change of shape of the characteristic as well as a shift of the pressure rise peak towards lower mass flow rates is visible. Due to the small injection mass flow rate of 2.2%, which is necessary to obtain stable seeding for PIV measurements, the gain in stalling mass flow is not very pronounced. More significant improvements could be achieved with higher injection mass flow rates, as was shown in Hiller et al. [5].

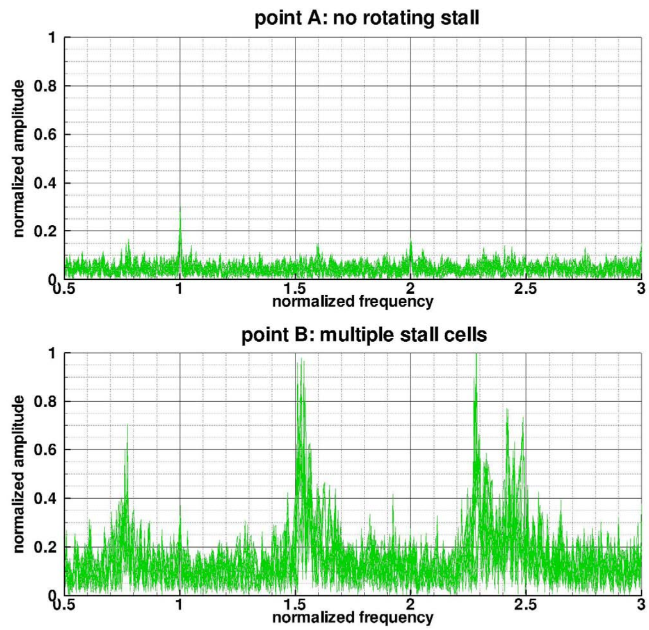

Fig. 7 Power density spectra of wall static pressure measurements at two throttling points

Additionally to the stage characteristics, points where PIV measurements were conducted are outlined in Fig. 6. As can be seen, a near stall point was chosen, which allowed for investigation of phenomena related to the onset of stall. Comparable conditions between measurements with and without injection were ensured by adjusting the same reduced inlet mass flow rate in both cases.

Rotor behavior without fluid injection

The picture gained by inspection of the front stage behavior, using stage characteristics and wall static pressure measurements, is now completed by looking at PIV measurements. As was mentioned at the beginning of this section, the position of the light sheet for PIV measurements was chosen such that it intersects the tip leakage vortex, even at its lowest point, which is at 96% of the annulus height. However, backflow, which is present over the radial extend of the tip leakage jet is not captured because this would require a measuring plane closer to the annulus wall, at about 99% annulus height.

Referring to ideas presented in [10], the position of the tip leakage vortex is a measure for the loading of tip critical blades and rotating stall may be observed as soon as it spills over the leading edge of the adjacent blade. By the choice of the light sheet position depicted above, PIV is able to capture such a behavior. Fig. 8 shows both the velocity field in the absolute frame of reference as well as the magnitude of strain rate, defined as:

$$\left|\varepsilon\right| = \sqrt{\varepsilon_1^2 + \varepsilon_2^2}\ .$$

The velocity magnitude was normalized by the averaged speed of the main flow. The magnitude of strain rate was normalized by its maximum value.

Fig. 8 clearly shows the position of the tip leakage vortex in both plots, which is indicated by a dashed line for clarity. Its trajectory is considered as the connecting points of the maxima of normalized strain rate magnitude, an approach which was also used for all following pictures where the tip leakage vortex trajectory is shown. The vortex trajectory is already aligned with the rotor's inlet plane and spillage over the leading edge is visible. According to [10], this is an indication for the onset of rotating stall, which underlines the picture gained from inspection of stage characteristics. There it was shown that the operating point selected for PIV measurements is placed closely to throttling states where fully developed rotating stall was detected.

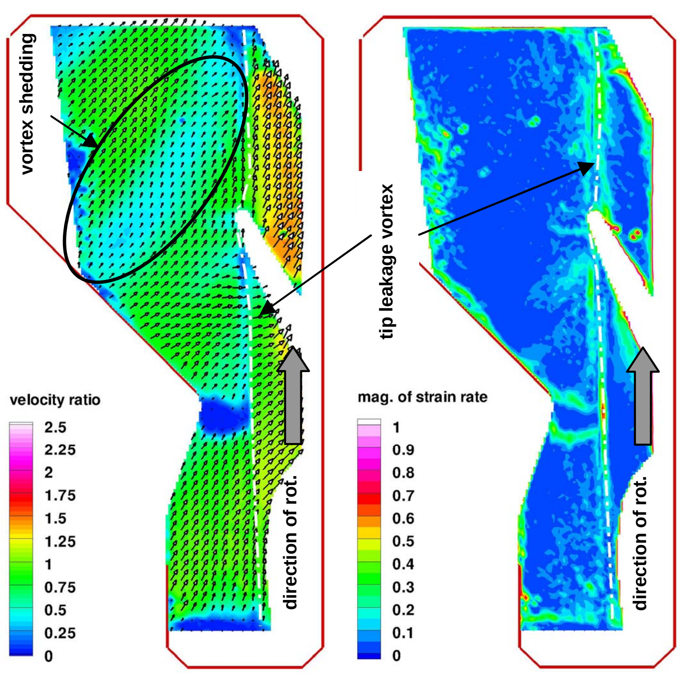

Fig. 8 Velocity ratio and normalized magnitude of strain rate for PIV results without tip injection

The velocity vector map of the inlet flow field appears to be very homogenous, neglecting parts shown in deep blue, where no information about the flow field could be gained due to zero correlation caused by laser reflections or contamination of the window. Only within a distinct region, which is marked with an open oval in Fig. 8, a decreased velocity magnitude compared to the rest of the flow field is visible. Inspection of a series of measurements at different phase angles Φ, i.e. at different relative rotor positions, showed that although the velocity defect's position was steady, the magnitude of velocity fluctuated. It thus can be concluded that vortices, which are shed from the IGV's trailing edge are discernable there.

Summarizing the findings made by inspection of measurement data without fluid injection, it can be concluded that the front rotor is highly loaded, particularly at the tip. Further throttling increases the loading, eventually leading to rotating stall. The tip leakage vortex is aligned with the rotor's leading edge at the mass flow rate selected for PIV measurements, underlining that rotating stall occurs. Apart from vortices shed from the IGV's tip the inflow field is steady and the rotor is not subject to highly varying inlet conditions in the relative frame of reference. This is a picture which changes drastically as soon as fluid injection is enabled.

Rotor behavior with fluid injection

With enabled fluid injection, discrete injection jets, evenly distributed around the circumference are generated. In the rotating frame of reference, this acts as an unsteady inflow condition to the rotor. The resulting unsteady interaction between a single jet and a blade will be depicted in this section.

Along with typical vortical structures inside the jet, the impact of the blade's potential field on the jet's trajectory and velocity distribution is discussed first. This is of particular importance for the design of an injection or recirculation system, as vortical structures inside the jet along with its deviation with respect to the main flow direction influence the available relative total pressure at the rotor leading edge inside the jet and therewith influence the radial extend of the jet. The chapter is concluded by a thorough discussion of the unsteady response of tip flow to the varying inflow conditions.

Impact of passage flow on the injection jet

According to the investigations presented in [11], among several other vortices, a counter rotating vortex pair appears inside the injection jet, which is the result of strong shear layers between the injected jet and the oncoming main flow. This vortex pair, which is the dominant flow feature of a jet in cross flow, influences the jet's shape and total pressure loss, both being crucial for the inflow conditions to the blade.

However, because PIV only provides information on a single plane, it is worthwhile to consider CFD results obtained from a simple three dimensional model and compare them to PIV results. The CFD model used for these purposes is depicted in Fig. 9. It consists of a rectangular flow channel on which an injection nozzle, comparable to the one used during rig testing, is placed. The model was gridded with a tetra-mesh and contains about 950000 nodes in total. Near-wall resolution was chosen such as to allow for y^+ values around 30. Total pressure and static pressure were prescribed at the inlet and outlet of the flow duct, respectively. Additionally, the flow was inclined with respect to the x-direction at the inlet, in order to produce the same cross-flow angle of approximately 20°, as was prevalent during rig testing. The injection jet was simulated by the injection nozzle placed on top of the duct having a total pressure boundary condition at its inlet. Boundary conditions were adjusted such as to obtain velocity ratios and an absolute main flow velocity as measured with PIV. Steady RANS-CFD calculations were then conducted using ANSYS CFX 12, employing the SST turbulence model. Although it is clear that the use of steady calculations along with a two-equation turbulence model does not fully capture the development of vortical structures inside the jet, other works, e.g. [11], have shown that the most dominant structures are covered reasonably well by such an approach.

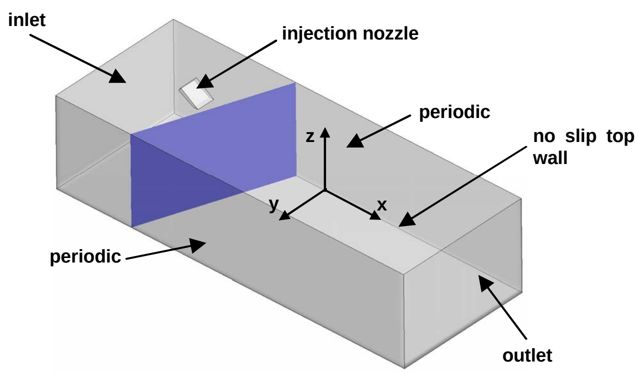

Fig. 9 CFD model used for comparison to PIV data

Fig. 10 compares contours of velocity ratio, i.e. velocity magnitude normalized with main flow velocity magnitude, along with velocity vectors obtained from CFD and from PIV.

PIV measurements were taken at the same radial position as used for Fig. 8, i.e. at a relative position of 96% annulus height at the measuring plane's midpoint. A phase angle was selected where only little interaction between rotor and injection jet was present. Concerning CFD results, a plane normal to the jet's trajectory was extracted, so as to capture velocity vectors normal to those gained from PIV. This slice is shown in blue in Fig. 9. Only velocity vectors projected onto the presented slice are given, to facilitate identification of vortical structures. By comparison of both results, vortical structures are identifiable.

At both edges of the injection jet distinct regions with augmented velocity (compared to the main flow), marked with the open ovals $\boxed{1}$ and $\boxed{3}$, appear. On the windward side of the jet $\boxed{3}$ the oncoming flow is diverted downwards under the injection jet which leads to an accelerated flow there. On the leeward side of the jet $\boxed{1}$ the main flow is accelerated again, which is visible by the augmented velocity. Strong shear layers at the jet's boundary to the main flow provoke the counter rotating vortex pair. Its aerodynamic background can be found in [11]. Inside the jet, the region where both vortices interact is clearly visible by low momentum fluid $\boxed{2}$.

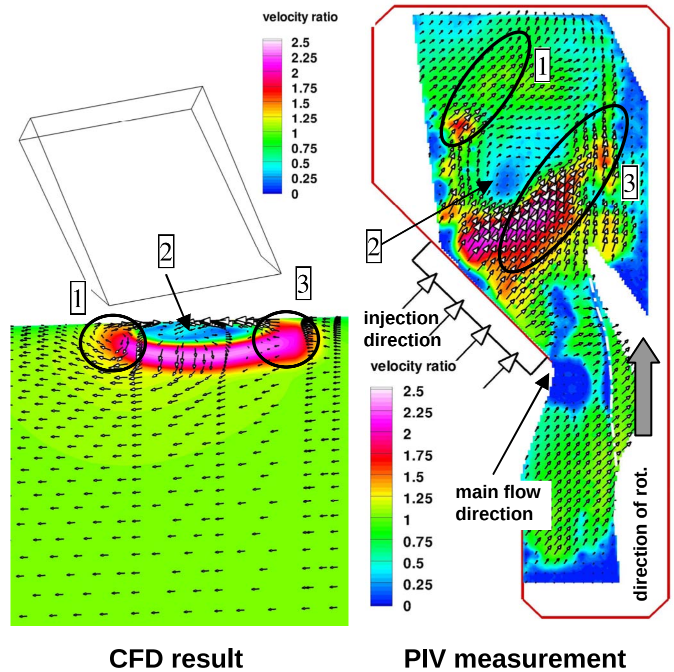

Fig. 10 Vortical structures inside the injection jet

Summarizing the aerodynamic features depicted in Fig. 10, it is obvious that due to strong interaction with the main flow, the injection jet is deformed and features distinct vortical structures. These vortices lead to total pressure loss, meaning that only a fraction of the total pressure provided at the nozzle's inlet is available at the rotor leading edge, which diminishes the available jet velocity. Since this is crucial when determining the inflow conditions to the rotor, this has to be accounted for when designing an injection nozzle.

Additionally to vortical structures inside the jet, which influence the jet's total pressure and trajectory, also the rotor's static pressure field has impact on the jet.

The left picture of Fig. 11 illustrates the wall static pressure field for a particular rotor position, as acquired by the array of 16 fast response pressure transducers. Static pressure was normalized with the corresponding ambient static pressure at the compressor's inlet. It is obvious that the suction peak of the rotor ranges far upstream the leading edge and penetrates the injection jet as well as the injection nozzles. The impact is twofold. First, the rotating static pressure field of the rotor induces periodically varying outlet conditions for the nozzle. If the nozzle operates choked, there is neither impact on mass flow rate nor on jet exit velocity. If a non-choked nozzle is used, a varying static pressure field provokes a varying jet exit velocity and mass flow. Hence, it is desirable to design nozzles which are choked over their operating range, because only then it is possible to determine the jet's total pressure and mass flow by flow conditions upstream of the nozzle.

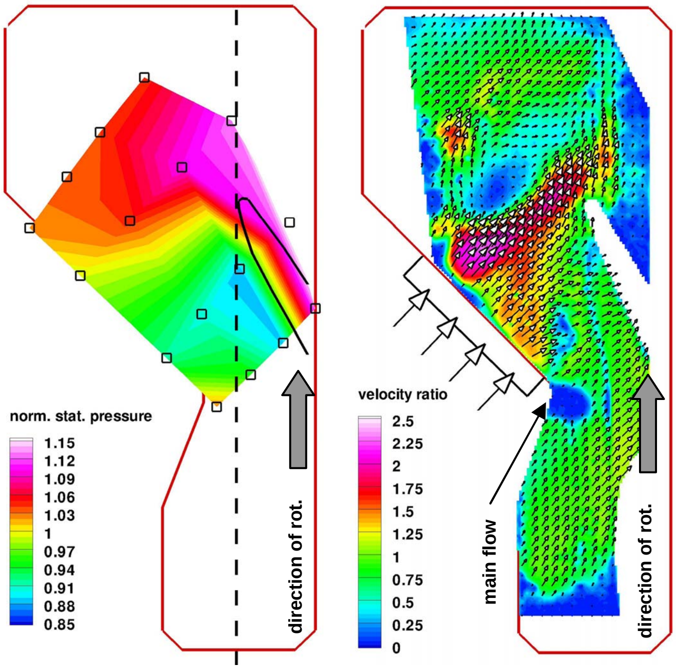

Fig. 11 Comparison between the blade's static pressure field and its velocity ratio field

Secondly, a distinct impact on the jet is visible by comparing the two pictures of Fig. 11. Due to the rotor's potential field the jet's trajectory and extension is altered. The jet is diverted in circumferential direction and its velocity diminishes due to the high pressure at the blade's pressure side passing the windward side of the jet.

This results in a changed incidence to the rotor compared to what was anticipated by the nozzle's extend and exit direction, because of the reduced velocity magnitude and the increased circumferential component. The effect of the blade's static pressure field on the jet may only be diminished if more axial distance between nozzle and leading edge was anticipated. Since this in turn leads to an increased distance the jet has to travel, its total pressure loss rises. It is therefore necessary to find an axial distance by pre-test CFD calculations where both effects are minimized.

Impact of the injection jet on the local tip flow

According to investigations on discrete tip injection (see introduction for references), its beneficial effect was linked to an unloading of the blade due to a decreased incidence and due to a shift of the tip leakage vortex, which reduced the threat of tip leakage vortex spillage. Circumferential averaging of altered inlet conditions as a result of discrete injection jets, in fact, gives a reduced incidence which would unload the blade. However, this approach treats the flow as axis-symmetric and assumes that passage flow follows the unsteady inlet conditions without any lag. Both, unsteady PIV results and comparison to open literature addressed in the following paragraphs show that this is an oversimplification.

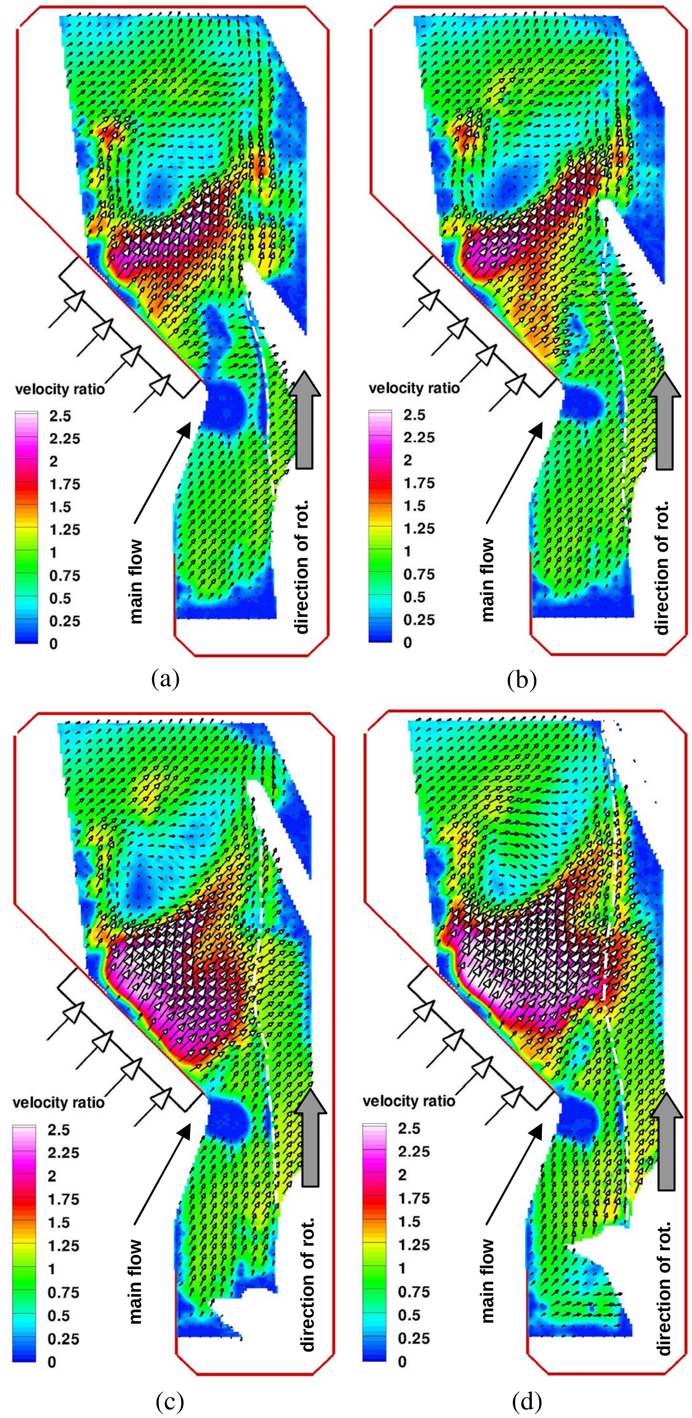

Fig. 12 Unsteady variation of tip leakage vortex trajectory, seen by unsteady snapshots

Results for different relative rotor positions, i.e. phase angles, are considered in the following, which aim to shed light on the unsteady variation of the tip leakage vortex as a function of the position between injection jet and blade. Fig. 12 depicts the velocity field, i.e. the magnitude of absolute velocity ratio along with vector maps of absolute velocity, for four different relative rotor positions.

The position of the tip leakage vortex is again deduced from the maxima of strain rate and marked with a white dashed line. Picture (a) in Fig. 12 shows the blade just entering the injection jet. Since it has passed a comparably long circumferential extend without any injection jet the local tip flow is similar to an undisturbed one. The tip leakage vortex is therefore virtually aligned with the rotor inlet plane. Its position is similar to the case without fluid injection, depicted in Fig. 8.

As soon as the blade is located inside the injection jet, as shown in picture (b), the origin of the tip leakage vortex at the blade's suction side is shifted inside the passage. This is caused by a decreased static pressure difference between pressure side and suction side as well as by an increased velocity along the blade.

Nevertheless, outside of the injection jet, i.e. upstream the jet in circumferential direction, the vortex's trajectory remains aligned with the rotor inlet plane, which shows that although its position is altered locally by the jet, it will interfere with the leading edge of the adjacent blade. As soon as the rotor leaves the injection jet, which is shown in picture (c), the incidence to the rotor increases again. At first, the tip leakage vortex remains inside the passage, which is caused by the strong injection jet acting on the vortex along the rotor's suction side. Looking at picture (d) it is obvious that the suction peak at the rotor's leading edge has already recovered, since the tip leakage vortex has moved forward towards the leading edge again. The only part of the vortex which remains inside the passage is the one under direct influence of the injection jet.

Summarizing these findings, it can be concluded that the loading at the blade's leading edge, which is crucial for the tip leakage vortex position, is only altered if the blade is under direct influence of the injection jet. The suction peak recovers rather quickly after leaving the injection jet and the trajectory of the tip leakage vortex aligns with the rotor's inlet plane virtually without any lag. Parts of the tip leakage vortex located outside of the injection jet remain unchanged. This shows that although the tip leakage vortex trajectory is altered locally, its overall position changes only slightly and is virtually similar to cases without tip injection. However, since a beneficial effect of tip injection is visible by inspection of the time averaged response of the rotor (e.g. by considering the change of operating behavior, as depicted in Fig. 6), other effects than a shift of the tip leakage vortex have to occur, which cause this behavior.

Due to the injection jet, the rotor passage is subject to unsteady non symmetric inflow conditions, which can easily be identified by comparing pictures (a) through (d) in Fig. 12. Symmetric inflow and flow-through, however, builds the basis of any steady theoretical passage flow model. Hence, concepts derived for steady passage flow are not applicable anymore.

Referring to concepts derived for unsteady compressor flow (see [12] and [13]), an airfoil in unsteady flow may be subject to higher incidence than in steady flow before stall occurs. Ericsson et al. [12] provides an explanation for that by showing that a finite time is needed for the flow to adapt to changed inlet conditions. The time needed is closely linked to the time a fluid particle needs to travel the distance between leading edge and trailing edge. This underlines the observation made above, where it was concluded that the suction peak at the leading edge recovers rather quickly. Fluid particles need a comparably short time to travel the distance from the stagnation point at the leading edge up to the suction side. As the pressure difference at the first few per cent of the chord drive the suction peak, it is obvious that it recovers virtually without any lag after leaving the injection jet.

Unlike the change of the suction peak, which happens quickly, a comparably long time is needed for the overall passage flow to adjust. This is the effect leading to an unloading of the blade in a time averaged sense, as observable by performance measurements.

Within the experiments described in this paper it was not possible to record the flow field all along the passage. More research, employing CFD calculations which complement measurements are needed, to get a thorough understanding of the unsteady flow features incorporated with the adaption of the overall passage flow. However, measurements presented in this paper already give a good indication that unloading of the blade and therewith stabilization of the compressor in an unsteady sense is caused by this unsteady adaption.

CONCLUSION

Complementing previous works on tip injection, which were focused on time averaged effects (best visible looking at stage and overall characteristics), the local unsteady flow at the rotor tip with and without tip injection was investigated in this paper. Particularly, the unsteady interaction between discrete injection jets and a transonic rotor was considered with the help of phase-locked PIV measurements and unsteady wall bounded pressure measurements. An adapted injection geometry as well as modifications to the compressor casing were needed, in order to get optical access to the flow field between rotor leading edge and the injection nozzles. Employing a measuring plane which intersects both the injection jet as well as the tip leakage vortex, the interaction between jet and blade could be recorded. Both, an influence of the blade's static pressure field on the injection jet as well as an influence of the jet on the rotor's flow field was clearly visible.

The blade's suction peak affected the nozzle's outlet conditions, causing varying static pressure there. Because choked nozzles were used, both the mass flow rate and exit velocity were independent from outlet conditions. Additionally, it could be shown that the blade's potential field led to a deviation of the jet's flow direction. Comparing PIV measurements and CFD results the interaction between rotor and jet as well as the appearance of strong vortices inside the injection jets were considered to be the main contributors to the jet's total pressure loss and deviation. Both were crucial for the flow conditions at the leading edge of the rotor and therefore have to be incorporated in tip injection design.

Unsteady interaction between the injection jet and the blade was best visible considering the position of the tip leakage vortex as a function of relative position between rotor and injection jet. Although a beneficial effect on both range extension and total pressure rise of the first rotor could be confirmed, which complemented findings of previous research works, an overall shift of the tip leakage vortex inside the passage was not visible. In fact, it was shown that the tip leakage vortex was only influenced locally, when penetrated by the injection jet. As only little time was needed for fluid particles to travel from the stagnation point up to the suction side, the suction peak at the blade's leading edge recovered virtually without any lag. Because the suction peak pressure difference was the main driver for the tip leakage vortex trajectory, only little influence on the vortex trajectory was observable from tip injection. As the distance between leading and trailing edge was significantly longer than the distance over the leading edge, it was concluded that the time needed for fluid particles to travel all along the chord was much longer than to travel over the leading edge. This led to the conclusion that the unsteady adaption of passage flow to the varying inflow conditions - rather than a shift of the tip leakage vortex – has to be the main reason for any beneficial effect of tip injection.

ACKNOWLEDGMENTS

The authors would like to thank the European Community to support the investigation, which was funded by the NEWAC project (No. FP6-030876).

REFERENCES

[1] Wilfert G., Sieber J., Rolt A., Baker N., Touyeras A., Colantuoni S.: New environmental friendly aero engine core concepts. Proceedings of ISABE 2007, ISABE-2007-1120

[2] Advisory Council for Aeronautics Research in Europe (ACARE): Strategic research agenda – vol. 2, 2004

[3] Suder K.L., Hathaway M.D., Thorp S.A., Strazisar A.J., Bright M.M.: Compressor stability enhancement using discrete tip injection, Proceeding of ASME Turbo Expo 2000, 2000-GT-650

[4] Cassina G., Beheshti B., Kammerer A., Abhari R.: Parametric study of tip injection in an axial flow compressor stage, Proceedings of ASME Turbo Expo 2007, GT2007-27403

[5] Hiller S.J., Matzgeller R., Horn W.: Stability enhancement of a multi stage compressor by air injection, Proceedings of ASME Turbo Expo 2009, GT2009-59868

[6] Raffel, M., Willert, C., Wereley, S., Kompenhans, J.: Particle Image Velocimetry, a practical guide (Second Edition), 2007, Springer Berlin Heidelberg, ISBN 978-3-540-72307-3

[7] Roesgen, T.: Optimal Subpixel Interpolation in Particle Image Velocimetry, Exp. Fluids (2003) 35: 252-256

[8] Westerweel, J., Scarano, F.: Universal Outlier Detection for PIV Data, Exp. Fluids (2005) 39: 1096-1100

[9] Westerweel, J.: Theoretical Analysis of the Measurement Precision in Particle Image Velocimetry, Exp. Fluids (2000) 29: Suppl. S3-S12

[10] Vo H.D., Tan C.S., Greitzer E.M.: Criteria for spike initiated rotating stall, Proceedings of ASME Turbo Expo 2005, GT2005-68374

[11] Sgarzi O., Leboeuf F.: Analysis of vortices in three-dimensional jets in a cross-flow boundary-layer, Proceedings of ASME Turbo Expo 1997, 97-GT517

[12] Ericsson L.E., Reding J.P.: Fluid mechanics of dynamic stall, part 1, Journal of fluids and structures, 1988, 2, 1-33

[13] Melick H., Simpkin W.E.: A unified theory of inlet/engine compatibility, AIAA paper, No.72-1115